Site-selective electronic structure of pure and doped $Ca_2O_3Fe_3S_2$

L. Craco,[1,2] B. Freelon,[3,4] A. M. Alafailakawi,[4] B. Karki,[4] and S. Leoni[5]
[1] *Instituto de Física, Universidade Federal de Mato Grosso, 78060-900 Cuiabá, Mato Grosso, Brazil*
[2] *IFW Dresden, Institute for Solid State Research, P.O. Box 270116, D-01171 Dresden, Germany*
[3] *Department of Physics, Massachusetts Institute of Technology, Cambridge, Massachusetts 02139, USA*
[4] *Department of Physics, University of Louisville, Louisville, Kentucky 40208, USA*
[5] *School of Chemistry, Cardiff University, Cardiff, CF10 3AT, United Kingdom*

(Received 12 April 2018; published 20 July 2018)

Using density functional dynamical mean-field theory we investigate the site-selective electronic structure of $Ca_2O_3Fe_3S_2$. We confirm that the parent compound with two distinct iron sites is a multiorbital Mott insulator similar to $La_2O_3Fe_2S_2$. Upon electron/hole doping, carrier localization is found to persist in the two active iron channels because the chemical potential lies in a gap structure with anisotropic and almost vanishing states near the Fermi energy. This emergent behavior stems from large electronic reconstruction caused by dynamical spectral weight transfer involving states with distinct d-shell occupancies and orbital character at low energies. We detail the implications of our microscopic analysis and discuss the underlying physics which will emerge in future experiments on $Ca_2O_3Fe_3S_2$.

DOI: 10.1103/PhysRevB.98.045130

I. INTRODUCTION

In recent years the large family of Fe-based compounds [1,2] has been the subject of intensive research after the discovery of high temperature superconductivity (high-T_c) in F-doped LaOFeAs [3]. It has emerged that these unconventional superconductors (both pnictides and chalcogenides) increasingly fall into the bad-metal category. In $SmFeAsO_{1-x}F_x$ [4], for example, suppression of superconductivity by high magnetic fields reveals a low temperature insulating behavior, similar to underdoped high-T_c cuprates [5]. Interestingly, in some cases superconductivity arises directly from a normal state with insulating-like [6,7] resistivity above T_c. Given telling similarities, along with notable differences, between the iron- and cuprate-based superconductors [8], an especially important issue has been to confirm whether the parent compounds are itinerant metals or if they lie in close proximity to a Mott metal-to-insulator transition [7,9]. Particularly interesting for the latter view are Fe-oxychalcogenides, which have been synthesized with various compositions [2,10–14], showing different degrees of electron localization.

A Mott insulator undergoes an electronic phase transition to a correlated metal at low temperatures [15]. The metallic behavior can vary from canonical Fermi to non-Fermi liquid depending on the degree of electronic correlation, disorder, and structural-induced changes in orbital polarization patterns. In all cases, the insulator-to-metal phenomenon is due to the development of a severely renormalized lattice coherence scale, driven by increasing relevance of electronic delocalization upon external perturbations like pressure and chemical substitution [15]. Optical and spectroscopic studies in 122-iron selenide superconductors [16], for example, show large-scale spectral weight transfer as function of temperature across the magnetic and superconducting phase instabilities, which is a fingerprint of Mottness [17].

In this context, finding insulating and antiferromagnetically ordered ground states in layered Fe-oxychalcogenides [11,12,14,18,19] is relevant, since it confirms theoretical suggestions that Mott-insulating parent compounds in the Fe-superconducting systems could be found by increasing the ratio of the interaction to hopping beyond a critical value for a Mott transition [20]. The Fe-oxychalcogenides [2] thus help to sharpen the fundamental debate [21] on the degree of electronic correlations in Fe-based superconductors in general. However, finding Mott electrons with different degrees of activation energies [11–14,18] suggests strong multiorbital (MO) electronic localization in this material class. In contrast to Fe-based superconductors, the consequences of Mottness (or the proximity to a insulator-metal transition) upon external perturbations in the Fe-oxychalcogenides has not received the theoretical attention it deserves. This is even more important when the Mott transition is unconventional in nature, as shown here in $Ca_2O_3Fe_3S_2$ where carrier localization persists on different Fe channels upon doping. Thus, following earlier studies on Fe-oxychalcogenides [22,23], we use the local density approximation plus dynamical mean-field theory (LDA+DMFT) [24] to study the role played by sizable MO electron-electron interactions in the Fe $3d$ shells of $Ca_2O_3Fe_3S_2$. As shown below, all five $3d$-bands of two distinct Fe sites (*Site 1, Site 2*) must be kept in order to satisfactorily resolve the site-selective Mott localization and bad-metallic regimes obtained, respectively, for pure and doped $Ca_2O_3Fe_3S_2$. In MO Mott insulators, sizable electronic correlations drive new physical effects from (electron/ hole) doping. They can induce a pseudogap regime, where the chemical potential lies in an energy region of vanishing density of states (DOS) near the Fermi energy (E_F) [25], or orbital-selective incoherent states, naturally yielding coexistent insulating and bad-metallic states as in cuprates [26] and Fe-pnictide superconductors [27]. In this work, we also use our results to discuss the influence of Mottness in lightly

2469-9950/2018/98(4)/045130(7)

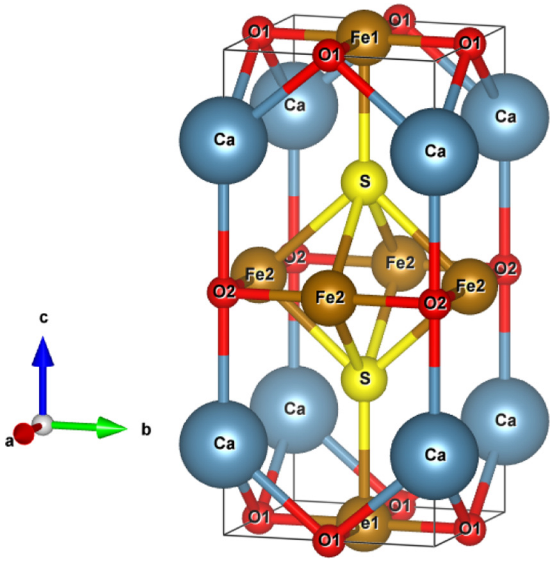

FIG. 1. The three-dimensional crystal structure of $Ca_2O_3Fe_3S_2$. Notice the two distinct iron sites.

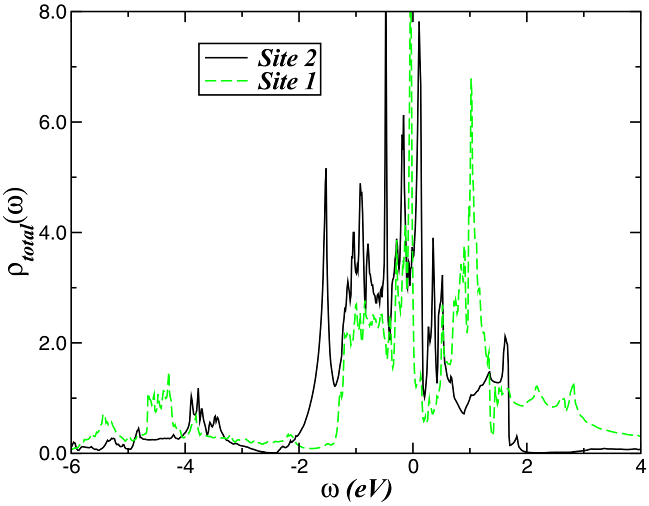

FIG. 2. LDA site-resolved, total density of states (DOS) of paramagnetic $Ca_2O_3Fe_3S_2$. Notice the transfer of spectral weight from valence to conduction band at *Site 1* compared to *Site 2* due to changes in crystal fields on different layers, inducing an Fe^{3+} oxidation state at *Site 1*.

doped $Ca_2O_3Fe_3S_2$, providing specific predictions which can be tested in future experiments.

II. RESULTS AND DISCUSSION

The crystal structure of $Ca_2O_3Fe_3S_2$ (space group $P4/mmm$) is built from alternate stacking of antiperovskite-like $[Ca_2FeO_2]^{2+}$ layers and $[Fe_2OS_2]^{2-}$ building blocks along the c axis [13], as shown in Fig. 1. Similar to the $Na_2Fe_2OSe_2$ oxychalcogenide Mott insulator [22], in the Fe_2OS_2 unit, the Fe^{2+} (d^6 electronic configuration) ions are located between oxygen atoms, forming a square-planar layer, which is an anticonfiguration with respect to the CuO_2 layer of high-T_c cuprates. As seen in Fig. 1, the two-dimensional $[CaFeO_2]^{2+}$ layers contain FeO_2 planar sheets separated from the $[Fe_2OS_2]^{2-}$ layers by Ca ions. The Fe ions (*Site 2*) in the $[Fe_2OS_2]^{2-}$ blocks are sixfold-coordinated by two O ions and four S ions, forming an FeO_2S_4 octahedron. Extant refinement of structural data for the individual sites of $Ca_2O_3Fe_{2.6}S_2$ revealed that the Fe sites at the planar layer (*Site 1*) are fully occupied, while at *Site 2* the Fe ions are about 20% deficient in this vacancy ordered compound.

To explore the site-selective electronic structure of the $Ca_2O_3Fe_3S_2$ parent compound, self-consistent band structure calculations were performed using the linear muffin-tin orbital (LMTO) method [28] in the atomic sphere approximation as implemented in PY LMTO computer code [29]. The Perdew-Wang parametrization [30] was used to construct the exchange correlation potential within LDA. The total density was converged on a grid of 819 irreducible k points, and the radii of the atomic spheres were chosen as $r_{Ca} = 3.57$ a.u., $r_O = 1.97$ a.u., $r_{Fe} = 2.45$ a.u., $r_S = 3.12$ a.u. in order to minimize their overlap. The LDA calculation we performed using the cell parameter values reported elsewhere for the $Ca_2O_3Fe_3S_2$ parent compound [13].

Our results in Figs. 2 and 3 confirm that similar to Fe-based superconductors the active electronic states involve Fe $3d$ carriers. A sizable enhancement of the average LDA bandwidth (W) relative to that of $La_2O_3Fe_2S_2$ [23] due to short Fe-Fe bonds [13] is obtained. As shown previously, $La_2O_3Fe_2S_2$ is a narrow band-gap Mott insulator [23,31], and the significantly larger on-particle bandwidth for $Ca_2O_3Fe_3S_2$ naturally implies proximity to metallization. Site- and orbital-driven anisotropies in the LDA band structure are also clearly manifested in Fig. 3. At *Site 2* the orbital-resolved DOS show similar features as found for $La_2O_3Fe_2S_2$, a result consistent with the Fe^{2+} oxidation state with six electrons in the Fe $3d$ shell. On the other hand, interesting deviations are seen for the xz, yz, xy and the $x^2 - y^2$ orbitals of *Site 1*, albeit less pronounced in the latter case. Due to changes in the crystal-field splittings the electronic states at *Site 1* are transferred to energies about E_F, severely renormalizing the LDA orbital occupancies compared to *Site 2*, promoting an Fe^{3+} valence state (d^5 electronic configuration) with enhanced orbital polarization. Thus, we attempt to address the following question: How do electron-correlations change from d^6 to d^5 electronic configuration? Typically, going from a partially to a half-filled $3d$ electron shell, electron correlation effects are expected to increase [32]. Here it is shown that this scenario holds true for $Ca_2O_3Fe_3S_2$. Additionally, as common to Fe-oxychalcogenides [22,23] and peculiar to the Fe-based superconductors, strong crystal-field splitting effects lift the xz, yz orbitals' degeneracy, leaving an antiferromagnetically ordered state at low temperatures [13] without tetragonal-to-orthorhombic structural phase transition or orbital nematic instabilities. It thus follows that the novelties found in Fe-based superconductors [33], relating to electronic nematic instabilities in the tetragonal phase near the borderline of structural and magnetic transitions, will not play an active role in $Ca_2O_3Fe_3S_2$: Only spin nematic phase fluctuations [34] are expected to be seen across the magnetic phase transition of $Ca_2O_3Fe_3S_2$ at low temperatures.

Currently, the theoretical microscopic understanding of $Ca_2O_3Fe_3S_2$ is restricted to LDA and LDA+U calculations [13]. Specifically, these *ab initio* density functional

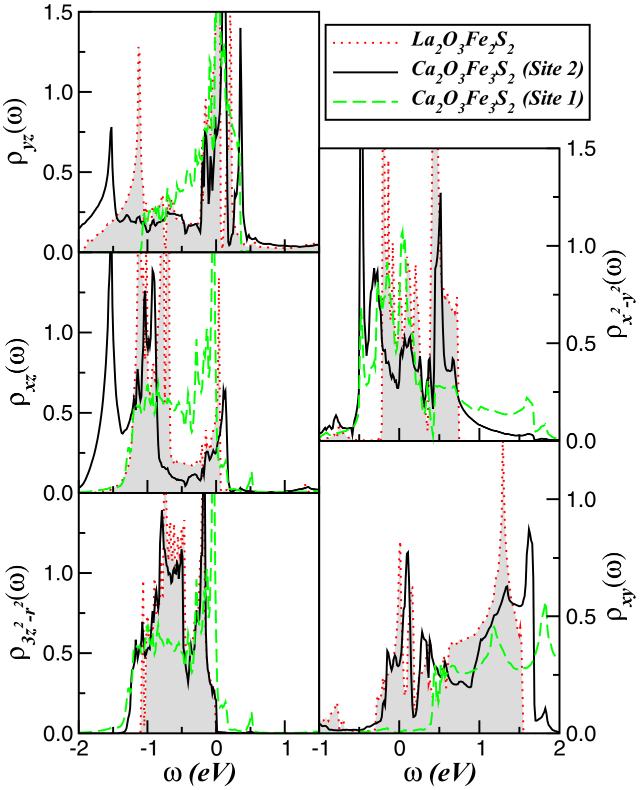

FIG. 3. Site- and orbital-resolved LDA DOS for the Fe $3d$ orbitals of $Ca_2O_3Fe_3S_2$. Results for $La_2O_3Fe_2S_2$ parent compound are shown for comparison. Notice the site-selective nature of the electronic and the broad bands in the LDA DOS of $Ca_2O_3Fe_3S_2$ as compared to $La_2O_3Fe_2S_2$.

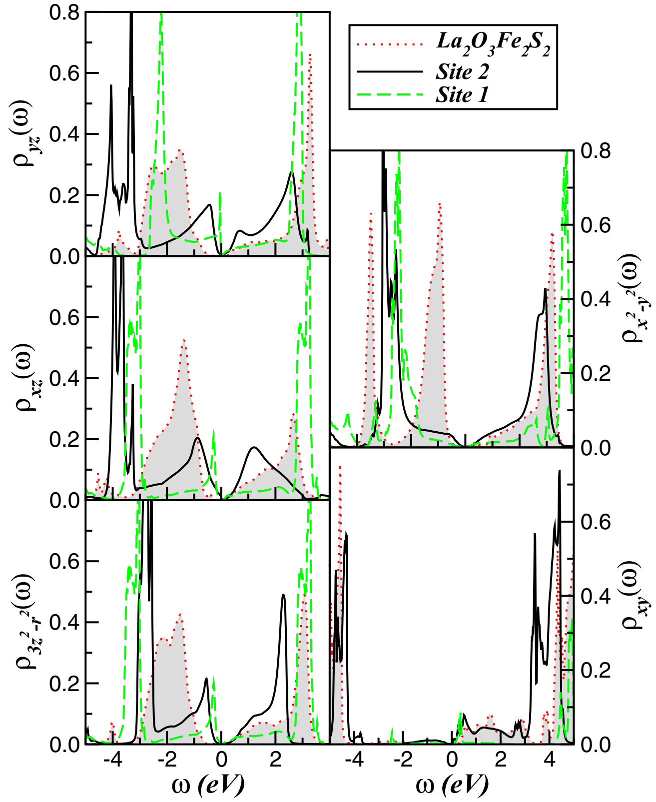

FIG. 4. LDA+DMFT ($U = 5.0$ eV, $J_H = 0.7$ eV) spectral functions for the Fe $3d$ orbitals at *Sites 1* and *2* of $Ca_2O_3Fe_3S_2$. Notice the enhanced electronic localization at *Site 1* compared to *Site 2* as expected for half-filled correlated electron systems. Compared to LDA results, also worth noticing is the reduced orbital polarization due to sizable U'-induced interorbital transfer of spectral weight.

calculations demonstrate that the chalcogen and oxygen p states lie well below E_F and are weakly hybridized with Fe $3d$ states. Hence, the most relevant electronic states near the Fermi energy for $Ca_2O_3Fe_3S_2$ derive from the Fe layers with almost direct Fe-Fe hopping. In previous works we undertook systematic LDA+DMFT studies of Fe-oxychalcogenides, showing that narrow-band Kondo-Mott localization [23] and orbital-selective localization-delocalization transition [22] can be understood within a single theoretical picture. Good semiquantitative agreement with experimental data of $La_2O_3Fe_2M_2$ ($M =$ Se, S) systems [23] serves as support to explore intrinsic, dynamical correlation effects in $Ca_2O_3Fe_3S_2$.

Although LDA+U provides reliable structural and magnetic ground state information of strongly correlated electron systems, it generically fails to capture the ubiquitous dynamical correlation effects in d-band compounds, and so cannot access normal state incoherence and the emergence of Hubbard satellites (local moments) at low and high energies. Combining LDA with DMFT is the state-of-the-art prescription for overcoming this problem [24]. Thus, as is common to Fe-based superconducting materials [35], within LDA the one-electron part of the Hamiltonian for $Ca_2O_3Fe_3S_2$ reads $H_0 = \sum_{\mathbf{k},a,\sigma} \epsilon_a(\mathbf{k}) c^\dagger_{\mathbf{k},a,\sigma} c_{\mathbf{k},a,\sigma}$, where $a = 3z^2-r^2, xz, yz, x^2-y^2, yz$ label the (diagonalized in orbital basis) five Fe $3d$ bands, which are the only ones we retain, since the non-$3d$-orbital DOS at *Sites 1* and *2* have negligible or no weight at E_F [13]. Here, the relevant inputs to our LDA+DMFT treatment for $Ca_2O_3Fe_3S_2$ are the LDA DOS for the five $3d$ orbitals at *Sites 1* and *2* shown in Fig. 3, the on-site Coulomb interaction U [13], the interorbital term $U' = U - 2J_H$, and Hund's coupling J_H. Based on this, at each Fe channel the correlated part of the many-body Hamiltonian for $Ca_2O_3Fe_3S_2$ is $H_{\rm int} = U \sum_{i,a} n_{i,a\uparrow} n_{i,a\downarrow} + \sum_{i,a\neq b} [U' n_{i,a} n_{i,b} - J_H \mathbf{S}_{i,a} \cdot \mathbf{S}_{i,b}]$. We choose values of $U = 5.0$ eV, $J_H = 0.7$ eV as employed in our earlier works for the Fe-oxychalcogenies [22,23]. Our parameter choice for the on-site Coulomb interaction is consistent with the U value used in Ref. [13] and the underlying view that Fe-oxychalcogenides are better regarded as strongly correlated electron systems [14]. We evaluated the many-particle Green's functions of the Hamiltonian $H = H_0 + H_{\rm int}$ above at *Sites 1* and *2* within LDA+DMFT [24], using MO iterated perturbation theory (MO-IPT) as impurity solver [36]. The DMFT solution involves replacing the lattice model by a self-consistently embedded MO-Anderson impurity model, the self-consistency condition requiring the local impurity Green's function to be equal to the local Green's function for the lattice. The full set of equations for the MO case can be found in Ref. [36].

In the case of undoped $Ca_2O_3Fe_3S_2$, our LDA+DMFT results at both Fe sites (see Fig. 4) exhibit a Mott insulating gap in the orbital-resolved one-particle spectral functions. Several noteworthy features are observed: (i) Although rather small within the xy band, the Mott gap is orbital dependent, i.e, intrinsically anisotropic. (ii) Carefully examining the orbital-resolved spectral functions of $La_2O_3Fe_2S_2$, one can see that the Mott phenomenon at *Sites 1* and *2* is weaker due to the presence of broad bands in $Ca_2O_3Fe_3S_2$ parent compound. As a result the orbital-selective Mott gap is smaller due to reduced effective Coulomb repulsion, which is controlled by the intrinsic U/W ratio. Interestingly, (iii) our results at *Sites 1* and *2* display a behavior which suggests strong similarities with the Fe-oxychalcogenide systems [22,23]. Namely, all orbitals are partially populated due to U'-induced dynamical interorbital entanglement [36]. As seen in Fig. 4, strong dynamical MO correlations originating from U, U' lead to sizable spectral weight redistribution over large energy scales and the formation of a severely reconstructed (compared to LDA) correlated electronic structure, with concomitant reduction of the orbital polarization patterns found in LDA. This behavior is characteristic of multiband Mott systems, where emergent upper and lower Hubbard bands are expected at high energies. These latter features are known to be related to coupled spin-orbital local moments defining a Mott insulator without long-range charge, orbital, or magnetic order.

Since there is no particle-hole symmetry in the bare electronic states of $Ca_2O_3Fe_3S_2$ (see Fig. 3), it is interesting to inquire what happens to the parent compound upon carrier (electron/hole) doping. In particular could selective localization characteristic of MO systems on the verge of Mott transition be found in future studies on doped $Ca_2O_3Fe_3S_2$? Indeed, the generic appearance of incoherent metallic states with low energy pseudogaps, and the instabilities of such states to unconventional orders in a wide variety of correlated electron systems [31,37], make this an important question. Our aim here is to build upon the strengths of MO correlated electronic structure calculations [24] to predict the effect of carrier doping on the two Fe sites of $Ca_2O_3Fe_3S_2$. In particular we will discuss a set of predictions which could be tested in future experimental work.

Figure 5 shows the changes in the correlated electronic structure upon electron and hole doping ($n \equiv 6 \pm \delta$) at *Site 2*. Similar to $Na_2Fe_2OSe_2$ [22], when δ increases to small negative values a selective-Mott state develops, in which the $3z^2 - r^2, xz, yz$, and $x^2 - y^2$ spectral functions show behavior of a Mott insulator with vanishing DOS at E_F. Meanwhile the xy orbital shows metallic behavior, characterized by the presence of incoherent in-gap states at E_F. On the other hand, enhanced metallicity is predicted for electron doped ($n = 6.2$) $Ca_2O_3Fe_3S_2$ where, in addition to the xy orbital, the xz, yz bands will also contribute to orbital-selective electronic transport and Fermi surface reconstruction within LDA+DMFT. Although the Mott gap in the $3z^2 - r^2$ and $x^2 - y^2$ bands is considerably reduced upon electron doping, strong localization is clearly visible in this orbital sector, as seen in Fig. 5. From the above observation it can be suggested that strong Mottness [25] and orbital-selective Mott physics coexist in the Fe^{2+} electronic channel. Since there is no particle-hole symmetry in the Fe^{3+} channel, it is interesting to inquire as to the effects of electron doping ($n \equiv 5 \pm \delta$) in this half-filled electronic reservoir. It is worth noticing here that electron-electron interactions are expected to reach their maximum at half-filling and to decrease away from this configuration [38]. This expected electronic behavior is consistent with our results in Fig. 4 where strong correlation fingerprints are found at *Site* 1 of the $Ca_2O_3Fe_3S_2$ parent compound. Therefore, it is of fundamental importance to see if electron/hole doping is qualitatively different at *Site 1* compared to *Site 2*, or whether incoherent non-Fermi-liquid behavior still emerges in the infrared region, or if Mott localization is favored. Figure 6 exhibits the answers to these fundamental questions. As seen, Mott localization persists in all orbitals at *Site 1* for electron doped $Ca_2O_3Fe_3S_2$. On the other hand, metallicity is found to be favored upon hole doping, and the $x^2 - y^2$, yz spectral functions show emergent spectral weight at E_F, while the $3z^2 - r^2$, xz, yz spectral functions now show pseudogap behavior. Hence, hole doping *Site 1* of $Ca_2O_3Fe_3S_2$ is predicted to lead to orbital-selective metallicity compared to its electron doped counterpart.

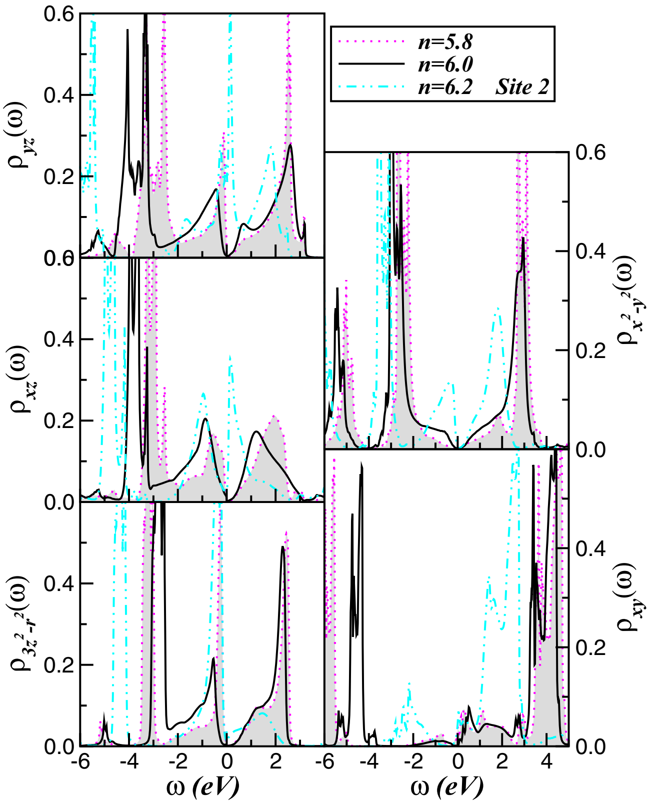

FIG. 5. Effect of electron/hole doping on the LDA+DMFT ($U = 5.0$ eV, $J_H = 0.7$ eV) spectral functions for the Fe $3d$ orbitals of $Ca_2O_3Fe_3S_2$ at *Site 2*. Notice the electron delocalization and the appearance of incoherent, pseudogapped shoulder quasiparticle resonances on different orbitals near the Fermi energy.

What is the origin of these orbital-selective features? In a MO system like the Fe-oxychalcogenides, strong (incoherent) scattering between different carriers in orbital states split relative to each other due to the specific crystal field and one-electron band fillings leads to two main effects: (i) It leads, via static-Hartree contributions (from the static part of the orbital-dependent self-energies) to orbital-dependent shifts of the d bands relative to each other; and (ii) strong dynamical correlations due to sizable U, U', J_H cause appreciable

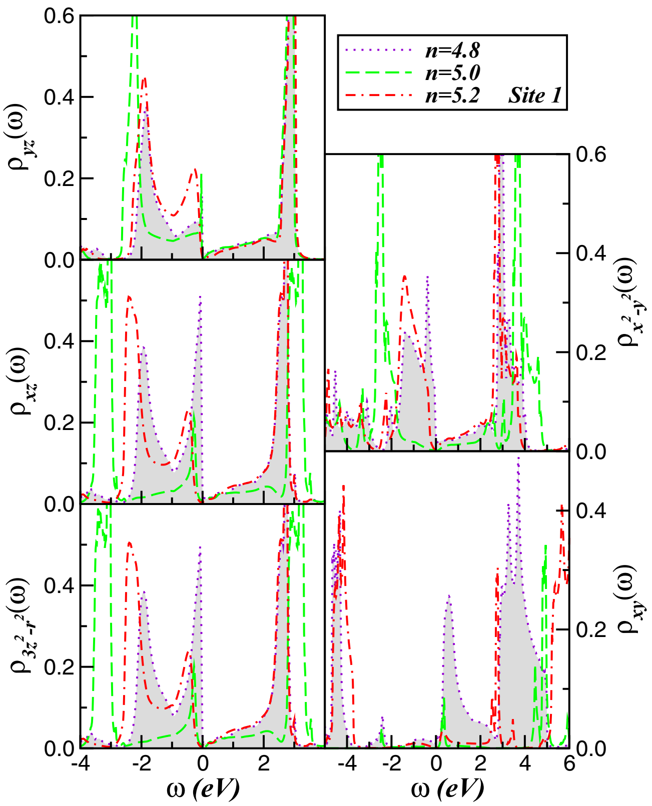

FIG. 6. Effect of electron/hole doping on the LDA+DMFT ($U = 5.0$ eV, $J_H = 0.7$ eV) spectral functions for the Fe 3d orbitals of $Ca_2O_3Fe_3S_2$ at *Site 1*. A particular feature is the Mott delocalization upon electron doping of the parent compound and appearance of incoherent quasiparticle shoulders near the Fermi energy for $n = 4.8$. Selective Mott-localization and pseudogap features are the fingerprints of strong electronic correlations in multiorbital systems close to half-filling.

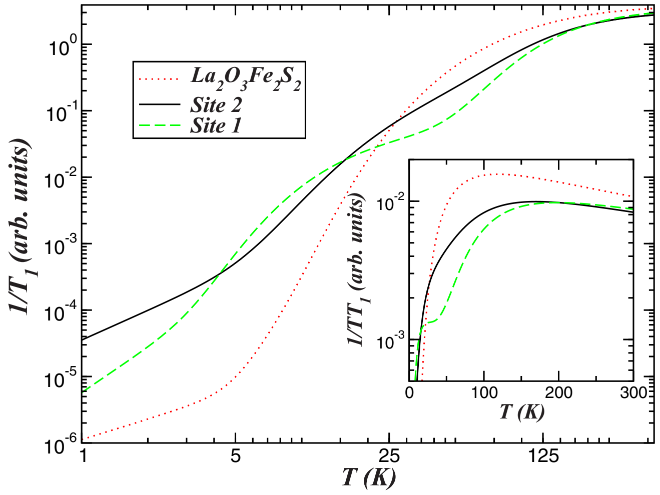

FIG. 7. Channel-selective temperature dependence of spin-lattice relaxation rate ($1/T_1$) for $Ca_2O_3Fe_3S_2$ obtained with LDA+DMFT spectral functions (for $U = 5.0$ eV and $J_H = 0.7$ eV). The inset shows the corresponding nuclear spin relaxation rate ($1/T_1T$) results. Notice the similar power-law behavior at both sites and the change in slope at low temperatures at *Site 2*, albeit less pronounced as compared to $La_2O_3Fe_2S_2$. This behavior marks the changes of multiorbital spin fluctuation modes as T is reduced.

spectral weight transfer over large energy scales, from high to low energy, upon carrier doping. This second feature leads to a drastic modification of the spectral lineshape as shown in Figs. 5 and 6. Microscopically, strong incoherent scattering, arising from coexistence of Mott-localized and bad-metallic states, leads to an almost complete suppression of the Fermi-liquid quasiparticles and the emergence of an incoherent spectrum, reminiscent of what is seen in cuprate oxides. Our results imply that doped $Ca_2O_3Fe_3S_2$ should be located in the pseudogap regime and the metallic state obtained by the filling-controlled Mott transition would be unconventional both at *Sites 1* and *2*. The origin of this emergent electronic state is the lattice orthogonality catastrophe [39] that occurs due to orbital-selective blocking of the coherent motion within LDA+DMFT due to sizable U' in the MO Hubbard model.

Armed with the above results, let us now discuss the implications of our results for future nuclear magnetic resonance (NMR) experiments. Here we recall that the spin-lattice relaxation rate ($1/T_1$) or the nuclear spin relaxation rate ($1/T_1T$) are directly computable using the DMFT propagators [40–42]. While $1/T_1$ quantifies the decay of the nuclear magnetic moments providing valuable information about the fluctuations of the electronic magnetic moments in the solid, $1/T_1T$ measures the slope of the imaginary part of the local spin susceptibility in the zero-frequency limit [42]. With these caveats in mind, in Fig. 7 we display the temperature dependence of local dynamical spin fluctuations by computing the NMR spin-relaxation rate $1/T_1$ as a function of T within the paramagnetic phase of $Ca_2O_3Fe_3S_2$ as done earlier for the $LaO_{1-x}FeAsF_x$ system [40]. Though experimental data do not exist yet, the T dependence of $1/T_1$ for the $Ca_2O_3Fe_3S_2$ parent compound is predicted to show similar site-dependent features in the nonmagnetically ordered state of $Ca_2O_3Fe_3S_2$. By assuming the hyperfine coupling constants for the two Fe-sites to be identical, a particularly interesting feature to be seen is the power-law behavior and the change in slope at low temperatures, albeit less pronounced as compared to $La_2O_3Fe_2S_2$, which marks the changes of MO spin fluctuation modes as T is reduced. If the nuclear spin relaxation at both Fe sites is driven by a single spin degree of freedom, one would expect the scaled relaxation rates to be equal [43]. However, the different relaxation rates we obtain for $Ca_2O_3Fe_3S_2$ indicates that both the magnitude and the T dependence of the two sites are not driven by the single relaxation mechanism, and that this relaxation mechanism is electronic state dependent. Enhanced Mott localization within the Fe^{3+} electronic channel tends to suppress local spin fluctuations due the formation of stronger localized moments in the half-filled shell. On the other hand the similarities in the relaxation rates seems to suggest that the Fe 3d spins fluctuate incoherently on both Fe sites, so that both of them may contribute to the relaxation similarly in future site-selective NMR experiments.

III. CONCLUSION

To summarize, we have used LDA+DMFT for a realistic two-channel Hubbard model with five active $3d$ bands at each channel to perform a detailed study of the paramagnetic Mott insulating state of $Ca_2O_3Fe_3S_2$. In particular, considering the Fe^{2+} ($S = 2$) and Fe^{3+} ($S = 5/2$) valence (spin) states intrinsic to this Fe-oxychalcogenide, we predict orbital-selective blocking of electrons and strong correlation fingerprints in the half-filled (Fe^{3+}) channel as an effect of multiorbital Hubbard correlations. Compared to $La_2O_3Fe_2S_2$, short Fe-Fe bonds intrinsic to $Ca_2O_3Fe_3S_2$ lead to decreased electron correlation through increasing bandwidth, an undoubtedly significant feature also present in the high-T_c FeSe/$SrTiO_3$ system [44]. Interesting as well is the emergent electronic behavior when we consider the effect of electron/hole doping in this two-channel system. We predict that localization or low-energy incoherence persists in doped $Ca_2O_3Fe_3S_2$ due to a lattice orthogonality catastrophe induced by orbital-selective Mottness. This orbital blocking phenomenon can be directly tested by a combination of future spectral, transport, and nuclear spin-lattice relaxation measurements. Such studies are called for, and should confirm or refute our predictions.

ACKNOWLEDGMENTS

L.C.'s work is presently supported by CNPq (Grant. No. 304035/2017-3). S.L. acknowledges support from the UK Research Council for using work in the paper that was undertaken by a student under Project No. EP/M50631X/1 as well as the DFG for support under the priority project SPP1415 and for a personal Heisenberg grant. S.L. also thanks ZIH Dresden and ARCCA Cardiff for computational resources. Via S.L.'s membership of the UK's HPC Materials Chemistry Consortium, which is funded by EPSRC (No. EP/L000202), this work made use of the facilities of ARCHER, the UK's National High-Performance Computing Service, which is funded by the Office of Science and Technology through EPSRC's High End Computing Programme.

[1] D. C. Johnston, Adv. Phys. **59**, 803 (2010); G. R. Stewart, Rev. Mod. Phys. **83**, 1589 (2011); K. Deguchi, Y. Takano, and Y. Mizuguchi, Sci. Technol. Adv. Mater. **13**, 054303 (2012); for more recent overviews on iron based superconductors see also M. K. Wu, P. M. Wu, Y. C. Wen, M. J. Wang, P. H. Lin, W. C. Lee, T. K. Chen, and C. C. Chang, J. Phys. D: Appl. Phys. **48**, 323001 (2015); Q. Si, R. Yu, and E. Abrahams, Nat. Rev. Mater. **1**, 16017 (2016).

[2] C. Stock and E. E. McCabe, J. Phys.: Condens. Matter **28**, 453001 (2016), and references therein.

[3] Y. Kamihara, T. Watanabe, M. Hirano, and H. Hosono, J. Am. Chem. Soc. **130**, 3296 (2008).

[4] S. C. Riggs, J. B. Kemper, Y. Jo, Z. Stegen, L. Balicas, G. S. Boebinger, F. F. Balakirev, A. Migliori, H. Chen, R. H. Liu, and X. H. Chen, Phys. Rev. B **79**, 212510 (2009).

[5] R. W. Hill, C. Proust, L. Taillefer, P. Fournier, and R. L. Greene, Nature (London) **414**, 711 (2001); Y. Ando, S. Komiya, K. Segawa, S. Ono, and Y. Kurita, Phys. Rev. Lett. **93**, 267001 (2004).

[6] T. J. Liu, X. Ke, B. Qian, J. Hu, D. Fobes, E. K. Vehstedt, H. Pham, J. H. Yang, M. H. Fang, L. Spinu, P. Schiffer, Y. Liu, and Z. Q. Mao, Phys. Rev. B **80**, 174509 (2009); Y. Mizuguchi, F. Tomioka, S. Tsuda, T. Yamaguchi, and Y. Takano, J. Phys. Soc. Jpn. **78**, 074712 (2009); M. H. Fang, J. H. Yang, F. F. Balakirev, Y. Kohama, J. Singleton, B. Qian, Z. Q. Mao, H. D. Wang, and H. Q. Yuan, Phys. Rev. B **81**, 020509 (2010).

[7] T. Yamauchi, Y. Hirata, Y. Ueda, and Kenya Ohgushi, Phys. Rev. Lett. **115**, 246402 (2015); H. Takahashi, A. Sugimoto, Y. Nambu, T. Yamauchi, Y. Hirata, T. Kawakami, M. Avdeev, K. Matsubayashi, F. Du, C. Kawashima, H. Soeda, S. Nakano, Y. Uwatoko, Y. Ueda, T. J. Sato, and K. Ohgushi, Nat. Mater. **14**, 1008 (2015).

[8] C. Ye, W. Ruan, P. Cai, X. Li, A. Wang, X. Chen, and Y. Wang, Phys. Rev. X **5**, 021013 (2015).

[9] Q. Si and E. Abrahams, Phys. Rev. Lett. **101**, 076401 (2008).

[10] C.-H. Wang, C. M. Ainsworth, S. D. Champion, G. A. Stewart, M. C. Worsdale, T. Lancaster, S. J. Blundell, H. E. A. Brand, and J. S. O. Evans, Phys. Rev. Mater. **1**, 034403 (2017).

[11] N. Ni, S. Jia, Q. Huang, E. Climent-Pascual, and R. J. Cava, Phys. Rev. B **83**, 224403 (2011).

[12] J. B. He, D. M. Wang, H. L. Shi, H. X. Yang, J. Q. Li, and G. F. Chen, Phys. Rev. B **84**, 205212 (2011).

[13] H. Zhang, X. Wu, D. Li, S. Jin, X. Chen, T. Zhang, Z. Lin, S. Shen, D. Yuan, and X. Chen, J. Phys.: Condens. Matter **28**, 145701 (2016).

[14] J.-X. Zhu, R. Yu, H. Wang, L. L. Zhao, M. D. Jones, J. Dai, E. Abrahams, E. Morosan, M. Fang, and Q. Si, Phys. Rev. Lett. **104**, 216405 (2010).

[15] M. Imada, A. Fujimori, and Y. Tokura, Rev. Mod. Phys. **70**, 1039 (1998).

[16] Z. G. Chen, R. H. Yuan, T. Dong, G. Xu, Y. G. Shi, P. Zheng, J. L. Luo, J. G. Guo, X. L. Chen, and N. L. Wang, Phys. Rev. B **83**, 220507(R) (2011); F. Chen, M. Xu, Q. Q. Ge, Y. Zhang, Z. R. Ye, L. X. Yang, J. Jiang, B. P. Xie, R. C. Che, M. Zhang, A. F. Wang, X. H. Chen, D. W. Shen, J. P. Hu, and D. L. Feng, Phys. Rev. X **1**, 021020 (2011).

[17] P. Phillips, T.-P. Choy, and R. G. Leigh, Rep. Prog. Phys. **72**, 036501 (2009).

[18] H. Kabbour, E. Janod, B. Corraze, M. Danot, C. Lee, M.-H. Whangbo, and L. Cario, J. Am. Chem. Soc. **130**, 8261 (2008).

[19] F. Han, X. Wan, B. Shen, and H.-H. Wen, Phys. Rev. B **86**, 014411 (2012).

[20] G. Baskaran, J. Phys. Soc. Jpn. **77**, 113713 (2008); R. Yu, J.-X. Zhu, and Q. Si, Phys. Rev. Lett. **106**, 186401 (2011).

[21] Q. Si, Nat. Phys. **5**, 629 (2009); M. M. Qazilbash, J. J. Hamlin, R. E. Baumbach, L. Zhang, D. J. Singh, M. B. Maple, and D. N. Basov, *ibid.* **5**, 647 (2009).

[22] L. Craco, M. S. Laad, and S. Leoni, J. Phys.: Condens. Matter. **26**, 145602 (2014).

[23] B. Freelon, Y. H. Liu, J.-L. Chen, L. Craco, M. S. Laad, S. Leoni, J. Chen, L. Tao, H. Wang, R. Flauca, Z. Yamani, M. Fang, C. Chang, J.-H. Guo, and Z. Hussain, Phys. Rev. B **92**, 155139 (2015).

[24] G. Kotliar, S. Y. Savrasov, K. Haule, V. S. Oudovenko, O. Parcollet, and C. A. Marianetti, Rev. Mod. Phys. **78**, 865 (2006).

[25] T.-P. Choy and P. Phillips, Phys. Rev. Lett. **95**, 196405 (2005).

[26] G. S. Boebinger, Y. Ando, A. Passner, T. Kimura, M. Okuya, J. Shimoyama, K. Kishio, K. Tamasaku, N. Ichikawa, and S. Uchida, Phys. Rev. Lett. **77**, 5417 (1996); K. Semba and A. Matsuda, *ibid.* **86**, 496 (2001).

[27] J. W. Simonson, K. Post, C. Marques, G. Smith, O. Khatib, D. N. Basov, and M. C. Aronson, Phys. Rev. B **84**, 165129 (2011); Y. Shiomi, S. Ishiwata, Y. Taguchi, and Y. Tokura, *ibid.* **84**, 054519 (2011).

[28] O. K. Andersen, Phys. Rev. B **12**, 3060 (1975).

[29] V. Antonov, B. Harmon, and A. Yaresko, *Electronic Structure and Magneto-Optical Properties of Solids* (Kluwer Academic, Dordrecht, 2004).

[30] J. P. Perdew and Y. Wang, Phys. Rev. B **45**, 13244 (1992).

[31] G. Giovannetti, L. de' Medici, M. Aichhorn, and M. Capone, Phys. Rev. B **91**, 085124 (2015).

[32] L. de' Medici, J. Mravlje, and A. Georges, Phys. Rev. Lett. **107**, 256401 (2011).

[33] See, for example, J. M. Ok, S.-H. Baek, D. V. Efremov, R. Kappenberger, S. Aswartham, J. S. Kim, J. van den Brink, and B. Büchner, Phys. Rev. B **97**, 180405 (2018), and references therein.

[34] B. Freelon, R. Sarkar, S. Kamusella, F. Brückner, V. Grinenko, S. Acharya, M. S. Laad, L. Craco, Z. Yamani, R. Flacau, I. Swainson, Y. Liu, H. Wang, J. Du, M. Fang, and H.-H. Klauss, arXiv:1708.01693.

[35] L. Craco, M. S. Laad, S. Leoni, and H. Rosner, Phys. Rev. B **78**, 134511 (2008); L. Craco and S. Leoni, Sci. Rep. **7**, 46439 (2017).

[36] L. Craco, Phys. Rev. B **77**, 125122 (2008).

[37] C. Pépin, Phys. Rev. B **77**, 245129 (2008); M. Neupane, P. Richard, Z.-H. Pan, Y.-M. Xu, R. Jin, D. Mandrus, X. Dai, Z. Fang, Z. Wang, and H. Ding, Phys. Rev. Lett. **103**, 097001 (2009); R. Yu and Q. Si, *ibid.* **110**, 146402 (2013); Z.-Y. Song, H. Lee, and Y.-Z. Zhang, New J. Phys. **17**, 033034 (2015).

[38] L. de Medici, G. Giovannetti, and M. Capone, Phys. Rev. Lett. **112**, 177001 (2014).

[39] C. M. Varma, Z. Nussinov, and W. van Saarloos, Phys. Rep. **361**, 267 (2002); N. Trivedi, Nat. Phys. **4**, 163 (2008), and references therein.

[40] L. Craco and M. S. Laad, Phys. Rev. B **80**, 054520 (2009).

[41] R. Žitko, Ž. Osolin, and P. Jeglič, Phys. Rev. B **91**, 155111 (2015).

[42] N. Dasari, N. S. Vidhyadhiraja, M. Jarrell, and R. H. McKenzie, Phys. Rev. B **95**, 165105 (2017).

[43] T. Goto, S. Nakajima, M. Kikuchi, Y. Syono, and T. Fukase, Phys. Rev. B **54**, 3562 (1996).

[44] S. Mandal, P. Zhang, S. Ismail-Beigi, and K. Haule, Phys. Rev. Lett. **119**, 067004 (2017).